CROSS-DOMAIN ADAPTATION FOR BIOMETRIC IDENTIFICATION USING PHOTOPLETHYSMOGRAM

Eugene Lee, Annie Ho, Yi-Ting Wang, Cheng-Han Huang, Chen-Yi Lee

Institute of Electronics
National Chiao Tung University
Hsinchu, Taiwan 30010
{eugenelet.ee06g, huang50213.ee04}@nctu.edu.tw cylee@si2lab.org

ABSTRACT

The adoption of biomedical signals such as photoplethysmogram (PPG) and electrocardiogram (ECG) for health parameter estimation on wearable devices is growing in tandem with the increase of attention in mobile healthcare. In our work, we use PPG signals extracted from PPG sensors which are used for biometric identification. A challenge for biometric identification using PPG signal is the variation in domain (placement of sensors, wavelengths, device variation, etc.). In this work, we propose the use of both unsupervised and semi-supervised adversarial learning techniques for cross-domain adaptation. As such algorithm will be deployed on wearable devices, we propose a compact model meeting tight memory footprint limitation. All experiments will be simulated using a public dataset (TROIKA) and our in-house dataset. By introducing a cross-domain adaptation approach across sensors, we observe an accuracy gain of 4.15% on our in-house dataset. The proposed semi-supervised learning technique gives an additional accuracy boost of 2.02%.

***Index Terms*—** Cross-domain adaptation, biometric identification, photoplethysmogram, deep learning

1. INTRODUCTION

With the increase in adoptation of wearable devices, the widespread of using photoplethysmogram (PPG) sensors for health parameter monitoring has become apparent. As PPG signals extracted from the human body contains biomarkers that is unique among different individuals, it contains important information hence it should only be accessible by authorized parties.

In our work, we study the applicability of PPG signals for biometric identification with the possibility of adding a layer of security on wearable devices. We propose the usage of a deep neural network (DNN) as an estimation model for biometric identification. The reasoning behind the usage of a DNN for this task is because of its resiliency to noise up to some level [1] and high adaptability to different environments when compared with a heuristic approach. DNN usually comes with high computational cost and has a lot parameters which does not fit into the category of wearable devices. To overcome this limitation, we adopt the design MobileNetV2 [2] into our network.

Besides improving the feasibility and reliability of biometric identification on wearable devices, we also study the applicability of our algorithm when there's a variation in PPG sensors. As a PPG sensor consist of a photodiode and light emitting diode (LED) manufactured with a specified spectral sensitivity and emitting wavelength respectively, a slight variation of such device is common. To replicate such variation, we introduce two LEDs of wavelength 850nm and 940nm paired with photodiodes of the same type. Our approach to this problem is to view signals from LEDs as data from different domains. We apply CycleGAN [3] as a cross-domain adaptation [4, 5] method to solve this problem.

Our paper is organized as follows. We first show the current advances in the field of biometric identification using PPG signals and existing cross-domain adaptation methods in Section 2. We next show our approach for cross-domain adaptation for biometric identification in Section 3. Results supporting the validity of our approach is shown in Section 4. Finally, we conlcude our paper in Section 5.

2. RELATED WORK

2.1. Biometric Identification

The use of biomedical signals for biometric identification is not novel and is an on-going research. Most widely used biomedical signal for biometric identification is electrocardiogram (ECG) signals studied by several works [6, 7]. In our work, our focus is on PPG signals due to its pervasive adoption in wearable devices. Earlier work like [8] uses handcrafted feature extractors, e.g. obtaining peak number, upward slope, downward slope and time interval of PPG signals as features. Using stored features as template, the identity of a PPG signal is found by finding its nearest neighbor where eu-

Work supported by MOST of Taiwan, project: 106-3011-E-009 -002

clidean distance is used as a metric. A follow-up work by the authors of [8] uses fuzzy logic for decision making [9]. As the handcrafted features obtained in the previous works wouldn't be consistent, a more statistical approach for feature extraction that uses linear discriminant analysis (LDA) is taken in [10]. One main drawback of their approach is the instability induced when the collecting condition is not controlled.

With the rise of deep learning, deep learning approaches have also been applied to this field. In [11], different statistical features are first extracted followed by clustering method to group different individuals and are classified using Deep Belief Network (DBN) [12] which is pretrained using Restricted Boltzmann Machine. Recently, a similar work coined as BiometricNet [13] is proposed which uses a DNN consisting of convolutional and long short-term memory (LSTM) layers. Their work poses the biometric identification problem as a one-vs-all (binary classification) problem while our work formulate it as a multi-class classification problem.

2.2. Cross-Domain Adaptation

The problem of cross-domain adaptation exist in multiple research domain and is commonly applied to vision related tasks. One notable work is Deep Domain Confusion [14] which is proposed for semi-supervised and unsupervised learning. They simultaneously optimize for both domain invariance and classification. In their work, a domain confusion loss based on maximum mean discrepancy (MMD) [15] is adopted to calculate the domain distance. A follow-up work [16] proposes the use of task correlation and replaces MMD with a domain classifier to improve cross-domain adaptation. Another notable work is CycleGAN [3] where a thorough introduction will be given in Section 3.2.

3. METHOD

In our work, data from two domains ($\mathcal{D}_\text{A}$ and $\mathcal{D}_\text{B}$) are acquired using sensors of different wavelength placed on the finger of the subject. Data acquired from $\mathcal{D}_\text{A}$ and $\mathcal{D}_\text{B}$ are denoted as $\boldsymbol{x}_\text{A}$ and $\boldsymbol{x}_\text{B}$ with its corresponding identity as $\boldsymbol{y}_\text{A}$ and $\boldsymbol{y}_\text{B}$ respectively. The number of identity (classes) is denoted as C and is one-hot encoded.

3.1. Biometric Identification

For biometric identification using PPG signals, a deep neural network is used to model mapping from an input signal (PPG) to the identity of an individual. The mapping function is known as a classifier denoted as $\mathcal{C}$. $\mathcal{C}$ is designed to be lightweight, easing the portability to wearable devices. Our architecture is based on MobileNetV2 [2] hence we name it PPG-MobileNet and show the architecture of $\mathcal{C}$ in Table 1. Since our model deals with one-dimensional data, all two-dimensional convolutional layers are converted to one-dimensional convolutional layers. This conversion also applies to depthwise separable layers found in bottleneck residual blocks as shown in Table 2.

Table 1: Architecture of PPG-MobileNet based on MobileNetV2 [2]. Note that our architecture differs from [2] where no bottleneck layers are repeated.

Input	Operator	t	c	s
100×1	conv1d	-	32	1
100×32	bottleneck	1	16	1
100×16	bottleneck	6	24	2
50×24	bottleneck	6	32	2
25×32	bottleneck	6	64	2
12×64	bottleneck	6	96	1
12×96	bottleneck	6	160	1
12×160	conv1d	-	512	1
1×512	conv1d	-	C	1

Table 2: Bottleneck residual block from [2] that transforms c to c' channels, with stride s, kernel size k and expansion factor t.

Input	Operator	Output
$w \times c$	conv1d ($k = 1$), ReLU	$w \times tc$
$w \times tc$	dwise ($k = 3$, s=s), ReLU	$\frac{w}{s} \times tc$
$\frac{w}{s} \times tc$	linear conv1d ($k = 1$)	$\frac{w}{s} \times c'$

The goal of our work is to apply a classifier trained using data from $\mathcal{D}_\text{B}$ to data from $\mathcal{D}_\text{A}$. The resulting classifier is denoted as $\mathcal{C}_\text{B}$ (subscript denotes the domain the classifier is trained on) and this training process is illustrated in Fig. 1a. Cross-domain inference (inference using data from $\mathcal{D}_\text{A}$ using classifier trained on $\mathcal{D}_\text{B}$) is shown in Fig. 1b.

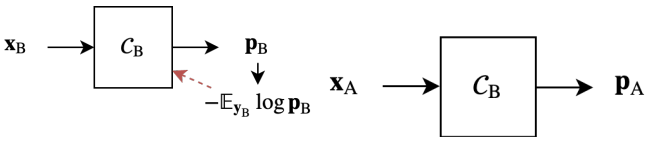

(a) Training using data from domain B. Red dashed line depicts the flow of gradient.

(b) Inference using data from domain A on model trained using data from domain B.

Fig. 1: A classifier modeled by a deep neural network will be used for biometric identification. (a) shows the training of the classifier using data from domain B only. (b) uses a classifier trained using data from domain B for the inference of data from domain A.

3.2. Unsupervised Cross-Domain Adaptation

To translate data across domains, we adopt a one-dimensional and simplified version of the adversarial architecture found in

CycleGAN [3]. The role of CycleGAN is to perform unpaired translation across domains in an unsupervised fashion. The importance of unpaired translation for biomedical signals in particular is the presence of phase difference between signals if they are collected at a different time instance. An unsupervised unpaired translation approach is highly suitable for biomedical signals like PPG because of the abundance and ease in collection of such signals.

The design of CycleGAN consists of two GANs with an additional consistency loss. The adversarial loss [17] is adopted for the training of GAN. Using the translation from $\mathcal{D}_\mathrm{A}$ to $\mathcal{D}_\mathrm{B}$ as an example, we have:

$$\mathcal{L}_{\mathrm{GAN}}(G_\mathrm{B}, D_\mathrm{B}, \mathcal{D}_\mathrm{A}, \mathcal{D}_\mathrm{B}) = \mathbb{E}_{\boldsymbol{x}_\mathrm{B}\sim\mathcal{D}_\mathrm{B}}[\log D_\mathrm{B}(\boldsymbol{x}_\mathrm{B})] + \mathbb{E}_{\boldsymbol{x}_\mathrm{A}\sim\mathcal{D}_\mathrm{A}}[\log(1 - D_\mathrm{B}(G_\mathrm{B}(\boldsymbol{x}_\mathrm{A})))]. \quad (1)$$

Here, the mapping function $G_\mathrm{B} : \mathcal{D}_\mathrm{A} \rightarrow \mathcal{D}_\mathrm{B}$ maps data across domains and D_B is a discriminator that penalties $G_{\mathrm{A}\rightarrow\mathrm{B}}$ if the domain of the translated data drifts away from the domain of the data originating from $\mathcal{D}_\mathrm{B}$.

As there are infinite mappings between domains, a cycle consistency loss is introduced to reduce the space of possible mapping functions. The cycle consistency loss is given as:

$$\mathcal{L}_{\mathrm{cyc}}(G_\mathrm{A}, G_\mathrm{B}) = \mathbb{E}_{\boldsymbol{x}_\mathrm{A}\sim\mathcal{D}_\mathrm{A}}[||G_\mathrm{A}(G_\mathrm{B}(\boldsymbol{x}_\mathrm{A})) - \boldsymbol{x}_\mathrm{A}||_1] + \mathbb{E}_{\boldsymbol{x}_\mathrm{B}\sim\mathcal{D}_\mathrm{B}}[||G_\mathrm{B}(G_\mathrm{A}(\boldsymbol{x}_\mathrm{B})) - \boldsymbol{x}_\mathrm{B}||_1]. \quad (2)$$

The resulting objective is given as:

$$\begin{aligned}\mathcal{L}(G_\mathrm{A}, G_\mathrm{B}, D_\mathrm{A}, D_\mathrm{B}) =& \mathcal{L}_{\mathrm{GAN}}(G_\mathrm{B}, D_\mathrm{B}, \mathcal{D}_\mathrm{A}, \mathcal{D}_\mathrm{B}) \\ &+ \mathcal{L}_{\mathrm{GAN}}(G_\mathrm{A}, D_\mathrm{A}, \mathcal{D}_\mathrm{B}, \mathcal{D}_\mathrm{A}) \\ &+ \lambda\mathcal{L}_{\mathrm{cyc}}(G_\mathrm{A}, G_\mathrm{B}), \end{aligned} \quad (3)$$

where λ corresponds to the importance of of the cycle consistency loss. The learning of the generators and discriminators is given as:

$$G_\mathrm{A}^*, G_\mathrm{B}^* = \arg\min_{G_\mathrm{A}, G_\mathrm{B}} \max_{D_\mathrm{A}, D_\mathrm{B}} \mathcal{L}(G_\mathrm{A}, G_\mathrm{B}, D_\mathrm{A}, D_\mathrm{B}). \quad (4)$$

An illustration summarizing the training of CycleGAN for our application is shown in Fig. 2.

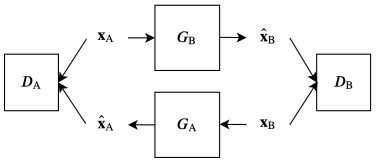

Fig. 2: Training of CycleGAN for unpaired translation of PPG data.

To translate a PPG signal from $\mathcal{D}_\mathrm{A}$ to $\mathcal{D}_\mathrm{B}$ to be classified by $\mathcal{C}_\mathrm{B}$, we used the trained G_B from (4) for cross-domain translation and feed the output of G_B to $\mathcal{C}_\mathrm{B}$ given as:

$$\boldsymbol{p}_\mathrm{A} = \mathcal{C}_\mathrm{B}(G_\mathrm{B}(\boldsymbol{x}_\mathrm{A})), \quad (5)$$

and is illustrated in Figure 3.

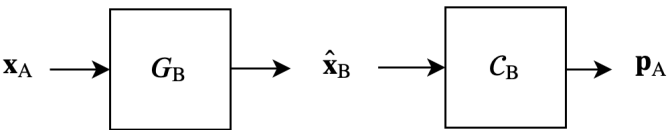

Fig. 3: Cross-domain inference using classifier $\mathcal{C}_\mathrm{B}$ trained using data from $\mathcal{D}_\mathrm{B}$ on data translated from $\mathcal{D}_\mathrm{A}$ to $\mathcal{D}_\mathrm{B}$ using G_B.

3.3. Semi-Supervised Cross Domain Adaptation

The labeling of data for biometric identification using biomedical signal does not take as much effort as image labeling, e.g. data collection can be continual for a single subject and is dependent on the collection interval. This motivates us to introduce partial data from $\mathcal{D}_\mathrm{A}$ to guide the training of G_B. To do so, we introduce a minor change on (3) where an additional *supporting loss* is introduced:

$$\mathcal{L}_{\mathrm{sup}}(G_\mathrm{B}, \mathcal{D}_\mathrm{A}) = -\mathbb{E}_{\boldsymbol{x}_\mathrm{A}, \boldsymbol{y}_\mathrm{A}\sim\mathcal{D}_\mathrm{A}} \log \boldsymbol{p}_\mathrm{A}(\boldsymbol{x}_\mathrm{A}) \quad (6)$$

$$= -\mathbb{E}_{\boldsymbol{x}_\mathrm{A}, \boldsymbol{y}_\mathrm{A}\sim\mathcal{D}_\mathrm{A}} \log \mathcal{C}_\mathrm{B}(G_\mathrm{B}(\boldsymbol{x}_\mathrm{A})). \quad (7)$$

The supporting loss (7) can be added to (3), giving us:

$$\begin{aligned}\mathcal{L}(G_\mathrm{A}, G_\mathrm{B}, D_\mathrm{A}, D_\mathrm{B}) =& \mathcal{L}_{\mathrm{GAN}}(G_\mathrm{B}, D_\mathrm{B}, \mathcal{D}_\mathrm{A}, \mathcal{D}_\mathrm{B}) \\ &+ \mathcal{L}_{\mathrm{GAN}}(G_\mathrm{A}, D_\mathrm{A}, \mathcal{D}_\mathrm{B}, \mathcal{D}_\mathrm{A}) \\ &+ \lambda\mathcal{L}_{\mathrm{cyc}}(G_\mathrm{A}, G_\mathrm{B}) \\ &+ \mathcal{L}_{\mathrm{sup}}(G_\mathrm{B}, \mathcal{D}_\mathrm{A}). \end{aligned} \quad (8)$$

Note that during the optimization of the new objective function (8), the parameters of $\mathcal{C}_\mathrm{B}$ are pretrained using $\mathcal{D}_\mathrm{B}$ and are frozen as illustrated in Fig. 4. This gives us the flexibility of swapping our generator whenever our model is deployed on another device while a trained classifier $\mathcal{C}_\mathrm{B}$ can be used directly. This has the benefit of a plug-and-play module and prevents the problem of catastrophic forgetting on our classifier.

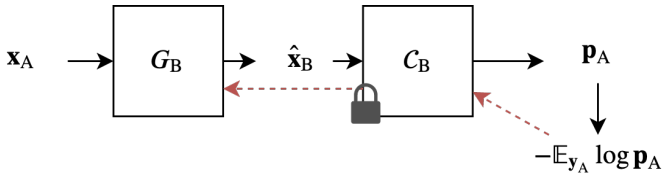

Fig. 4: Training of generator G_B is supported by gradient backpropagated from classifier $\mathcal{C}_\mathrm{B}$. The parameters of $\mathcal{C}_\mathrm{B}$ are frozen during the weight update process. Red dashed line depicts the flow of gradient.

4. EXPERIMENTS

To show the validity of our proposed methods, we use two datasets for simulation. The first is a public dataset known as

TROIKA dataset [18] which consists of two-channel PPG signals collected from 12 male subjects with ages ranging from 18 to 35. Two pulse oximeters with green LEDs of wavelength 515nm is embedded in a wristband which is used to collect PPG signals sampled at 125 Hz. The second is our private dataset collected using our in-house PPG sensor [19] which has two channels of different wavelengths (850nm and 940nm). PPG signals are collected from 10 subjects aging from 21 to 83 composed of 5 males and 5 females. PPG signal is collected from the subject's thumb with their arm relaxed. A total of 8 to 11 independent sequences are collected from each subject where a maximum of three sequences are collected a day spanning over several days. For sequences collected on the same day, a minimum of a 5 minutes interval between collections are taken to prevent high similarity between sequences to match the real use-case.

For training and validation set preparation for TROIKA dataset, we randomly subsample 24% of data for validation and the rest are used for training. Only data from the second PPG stream is used to train our classifier. For our in-house dataset, sequences are not joint as found in TROIKA which matches the real use-case. We split our training and validation data in a way where they do not originate from the same sequence. Approximately 30% of the sequences of each subject is used for validation and the rest for training.

Same pre-processing steps are applied for both dataset. We first apply a Butterworth band-pass filter of 5th order having the cut-off frequencies of 0.1Hz - 18Hz for TROIKA and 0.01Hz - 20Hz for our in-house dataset. The band-passed filter is then de-trended (restricted to be between -1 and 1) to ease the training of our network given as:

$$\hat{\boldsymbol{x}} = \frac{\boldsymbol{x} - \bar{\boldsymbol{x}}}{\max(\boldsymbol{x}) - \min(\boldsymbol{x})}. \tag{9}$$

For network training, PyTorch is used as our framework. We use Adam optimizer at a learning rate of 0.002 and batch size of 25 to train our classifier (both PPG-MobileNet and BiometricNet). For both datasets and classifiers, we train for 250 epochs. We compare the performance of our proposed architecture with BiometricNet only since BiometricNet is the current state-of-the-art architecture for biometric identification using PPG. Since only binary classification is used in BiometricNet [13], we show results for both multi-class and binary-class classification. Comparison results are shown in Table 3. From the results, we can see that our proposed network supersedes BiometricNet in all category with comparable model size and FLOPs as shown in Table 4. For multi-class classification, and increment of 9.2% and 24.81% in accuracy for our dataset and TROIKA dataset respectively can be observed.

We next show the application of CycleGAN for both unsupervised and semi-supervised cross-domain adaptation. The design of CycleGAN is similar to the original paper (using ResNet) where two-dimensional convolutional layers are reduced to one-dimensional. We use PPG-MobileNet as our classifier which attains an accuracy of 96.85% for this experiment. Note that the classifier weights are frozen and only the weights of CycleGAN are trained for this experiment. Convincing results are shown in Table 5 showing a 4.15% and 6.17% accuracy gain when unsupervised and semi-supervised adaptation are used respectively. We can see that there's still room for improvement as there's a gap of 5.41% in accuracy when compared to directly classifying samples from the original domain.

Table 3: Accuracy comparison between PPG-MobileNet and BiometricNet.

Dataset	Network	Accuracy (%)
Our Dataset	PPG-MobileNet	**95.68±0.24**
	BiometricNet [13]	86.48±0.41
TROIKA [18] (Binary-class)	PPG-MobileNet	**89.35±1.09**
	BiometricNet [13]	88.81±1.35
TROIKA [18] (Multi-class)	PPG-MobileNet	**69.46±0.51**
	BiometricNet [13]	44.65±0.49

Table 4: Comparison of model size and computation cost.

Network	Parameters (K)	FLOPs (M)
PPG-MobileNet	343.47	41.43
BiometricNet [13]	443.34	33.48

5. CONCLUSION

In our work, our contribution is two-fold. First, we propose a compact architecture for biometric identification using PPG with model size suitable for wearable devices. Second, we propose an unsupervised and a semi-supervised cross-domain adaptation method is applicable whenever there's a variation in the PPG sensor. Using both a public and an in-house dataset, accuracy gain is observed when compared with the current state-of-the-art network under the same experimental settings and network capacity. Our cross-domain adaptation approach is also proven to be effective.

Table 5: Accuracy comparison showing importance of cross-domain adaptation when different sensors are used.

Classifier's Input Domain	Accuracy (%)
Original Domain	96.85
Cross-Domain w/o any Adaptation	85.27
Cross-Domain w/ Unsupervised Adaptation	89.42±0.50
Cross-Domain w/ Semi-Supervised Adaptation	91.44±0.45

6. REFERENCES

[1] Samuel Dodge and Lina Karam, "Understanding how image quality affects deep neural networks," in *2016 eighth international conference on quality of multimedia experience (QoMEX)*. IEEE, 2016, pp. 1–6.

[2] Mark Sandler, Andrew Howard, Menglong Zhu, Andrey Zhmoginov, and Liang-Chieh Chen, "Mobilenetv2: Inverted residuals and linear bottlenecks," in *Proceedings of the IEEE Conference on Computer Vision and Pattern Recognition*, 2018, pp. 4510–4520.

[3] Jun-Yan Zhu, Taesung Park, Phillip Isola, and Alexei A Efros, "Unpaired image-to-image translation using cycle-consistent adversarial networks," in *Proceedings of the IEEE international conference on computer vision*, 2017, pp. 2223–2232.

[4] Sinno Jialin Pan, Xiaochuan Ni, Jian-Tao Sun, Qiang Yang, and Zheng Chen, "Cross-domain sentiment classification via spectral feature alignment," in *Proceedings of the 19th international conference on World wide web*. ACM, 2010, pp. 751–760.

[5] Mingsheng Long, Jianmin Wang, Guiguang Ding, Jiaguang Sun, and Philip S Yu, "Transfer joint matching for unsupervised domain adaptation," in *Proceedings of the IEEE conference on computer vision and pattern recognition*, 2014, pp. 1410–1417.

[6] Yongjin Wang, Foteini Agrafioti, Dimitrios Hatzinakos, and Konstantinos N Plataniotis, "Analysis of human electrocardiogram for biometric recognition," *EURASIP journal on Advances in Signal Processing*, vol. 2008, no. 1, pp. 148658, 2007.

[7] Adrian DC Chan, Mohyeldin M Hamdy, Armin Badre, and Vesal Badee, "Wavelet distance measure for person identification using electrocardiograms," *IEEE transactions on instrumentation and measurement*, vol. 57, no. 2, pp. 248–253, 2008.

[8] YY Gu, Y Zhang, and YT Zhang, "A novel biometric approach in human verification by photoplethysmographic signals," in *4th International IEEE EMBS Special Topic Conference on Information Technology Applications in Biomedicine, 2003.* IEEE, 2003, pp. 13–14.

[9] YY Gu and YT Zhang, "Photoplethysmographic authentication through fuzzy logic," in *IEEE EMBS Asian-Pacific Conference on Biomedical Engineering, 2003.* IEEE, 2003, pp. 136–137.

[10] Petros Spachos, Jiexin Gao, and Dimitrios Hatzinakos, "Feasibility study of photoplethysmographic signals for biometric identification," in *2011 17th International Conference on Digital Signal Processing (DSP)*. IEEE, 2011, pp. 1–5.

[11] Vasu Jindal, Javad Birjandtalab, M Baran Pouyan, and Mehrdad Nourani, "An adaptive deep learning approach for ppg-based identification," in *2016 38th Annual international conference of the IEEE engineering in medicine and biology society (EMBC)*. IEEE, 2016, pp. 6401–6404.

[12] Honglak Lee, Roger Grosse, Rajesh Ranganath, and Andrew Y Ng, "Convolutional deep belief networks for scalable unsupervised learning of hierarchical representations," in *Proceedings of the 26th annual international conference on machine learning*. ACM, 2009, pp. 609–616.

[13] Luke Everson, Dwaipayan Biswas, Madhuri Panwar, Dimitrios Rodopoulos, Amit Acharyya, Chris H Kim, Chris Van Hoof, Mario Konijnenburg, and Nick Van Helleputte, "Biometricnet: Deep learning based biometric identification using wrist-worn ppg," in *2018 IEEE International Symposium on Circuits and Systems (ISCAS)*. IEEE, 2018, pp. 1–5.

[14] Eric Tzeng, Judy Hoffman, Ning Zhang, Kate Saenko, and Trevor Darrell, "Deep domain confusion: Maximizing for domain invariance," *arXiv preprint arXiv:1412.3474*, 2014.

[15] Karsten M Borgwardt, Arthur Gretton, Malte J Rasch, Hans-Peter Kriegel, Bernhard Schölkopf, and Alex J Smola, "Integrating structured biological data by kernel maximum mean discrepancy," *Bioinformatics*, vol. 22, no. 14, pp. e49–e57, 2006.

[16] Eric Tzeng, Judy Hoffman, Trevor Darrell, and Kate Saenko, "Simultaneous deep transfer across domains and tasks," in *Proceedings of the IEEE International Conference on Computer Vision*, 2015, pp. 4068–4076.

[17] Ian Goodfellow, Jean Pouget-Abadie, Mehdi Mirza, Bing Xu, David Warde-Farley, Sherjil Ozair, Aaron Courville, and Yoshua Bengio, "Generative adversarial nets," in *Advances in neural information processing systems*, 2014, pp. 2672–2680.

[18] Zhilin Zhang, Zhouyue Pi, and Benyuan Liu, "Troika: A general framework for heart rate monitoring using wrist-type photoplethysmographic signals during intensive physical exercise," *IEEE Transactions on biomedical engineering*, vol. 62, no. 2, pp. 522–531, 2014.

[19] Eugene Lee, Tsu-Jui Hsu, and Chen-Yi Lee, "Centralized state sensing using sensor array on wearable device," in *2019 IEEE International Symposium on Circuits and Systems (ISCAS)*. IEEE, 2019, pp. 1–5.